Models of Voltage-Dependent Conformational Changes in NaChBac Channels

Yinon Shafrir, Stewart R. Durell, and H. Robert Guy
Laboratory of Cell Biology, CCR, National Cancer Institute, National Institutes of Health, Bethesda, Maryland 20892-5567

ABSTRACT Models of the transmembrane region of the NaChBac channel were developed in two open/inactivated and several closed conformations. Homology models of NaChBac were developed using crystal structures of Kv1.2 and a Kv1.2/2.1 chimera as templates for open conformations, and MlotiK and KcsA channels as templates for closed conformations. Multiple molecular-dynamic simulations were performed to refine and evaluate these models. A striking difference between the S4 structures of the Kv1.2-like open models and MlotiK-like closed models is the secondary structure. In the open model, the first part of S4 forms an α-helix, and the last part forms a 3_{10} helix, whereas in the closed model, the first part of S4 forms a 3_{10} helix, and the last part forms an α-helix. A conformational change that involves this type of transition in secondary structure should be voltage-dependent. However, this transition alone is not sufficient to account for the large gating charge movement reported for NaChBac channels and for experimental results in other voltage-gated channels. To increase the magnitude of the motion of S4, we developed another model of an open/inactivated conformation, in which S4 is displaced farther outward, and a number of closed models in which S4 is displaced farther inward. A helical screw motion for the α-helical part of S4 and a simple axial translation for the 3_{10} portion were used to develop models of these additional conformations. In our models, four positively charged residues of S4 moved outwardly during activation, across a transition barrier formed by highly conserved hydrophobic residues on S1, S2, and S3. The S4 movement was coupled to an opening of the activation gate formed by S6 through interactions with the segment linking S4 to S5. Consistencies of our models with experimental studies of NaChBac and K_v channels are discussed.

INTRODUCTION

Elucidation of the mechanisms by which voltage-gated channels open and close in response to voltage changes has been a major goal in membrane biophysics since the original experiments of Hodgkin and Huxley (1). When Noda et al. (2) cloned a voltage-gated sodium channel (Na_v), they identified six segments, S1–S6, that occur in each of four homologous repeats, and proposed that S4 forms the voltage sensor. Early models of the Na_v channel added to this picture by proposing the current standard transmembrane topology (3), and by identifying which segments form the selectivity filter, voltage sensor, inactivation gate, and several drug and toxin binding sites (4). New data were then incorporated into successive generations of atomically explicit models. Determination of the crystal structures of K^+ channels allows us to evaluate these models and, by implication, the methods used to develop them. Fig. 1, *A–C*, compares crystal structures of the voltage-sensing domain (VSD) of the KvAP (5) and Kv1.2/2.1 chimera (6) with the last *Shaker* model (7) we described before the determination of any K^+-channel crystal structure. Features of the *Shaker* model similar to those of the Kv1.2/2.1 crystal include the secondary structure, the order of the S1–S4 segments in the helical bundle, the tilt of S4 relative to the membrane, formations of specific salt bridges between positively charged side chains of *R3*, *R4*, *R5*, and *R6* on S4, and the negatively charged residues *E1*, *D2a*, *E2b*, and *D3* of S1–S3 (italics denote generic residue names and numbers applicable to all sequences; see Fig. 2), and locations of putative transition barrier residues (Fig. 1, *black*) of S1, S2, and S3.

Here we used similar methods and criteria to develop initial models of NaChBac channels. However, we now have the additional advantage of using crystal structures of homologous channels as templates. We also performed molecular-dynamic (MD) simulations of membrane protein embedded in a membrane, with water and ions on each side and in the pore, to refine and evaluate our models (see Methods in our accompanying study). These newer components of modeling should eliminate much of the ambiguity, and improve the models substantially.

Open-conformation structures and models still do not address how the VSD responds to voltage. Our group proposed (3) and has consistently advocated (4–9) the ''helical screw'' model, in which S4 rotates about and translates along its axis. When S4 moves outwardly or inwardly by one helical screw step, the *n*th residue moves to a position occupied by the ($n \pm 3$)th residue before the step; S4 rotates by ~60° about its axis, and translates ~4.5 Å along its axis during one step. Each helical screw step should contribute ~1 gating charge per helix. Subsequent measurements of gating currents in *Shaker* channels indicated that ~13 charges per channel cross the

Submitted April 15, 2008, and accepted for publication June 30, 2008.

Address reprint requests to H. Robert Guy, Laboratory of Cell Biology, CCR, National Cancer Institute, National Institutes of Health, 12 South Dr., Bethesda, MD 20892-5567. Tel.: 301-496-2068; Fax: 301-402-4724; E-mail: bg4y@nih.gov.

Editor: Francisco Bezanilla.

0006-3495/08/10/3663/14 $2.00

doi: 10.1529/biophysj.108.135335

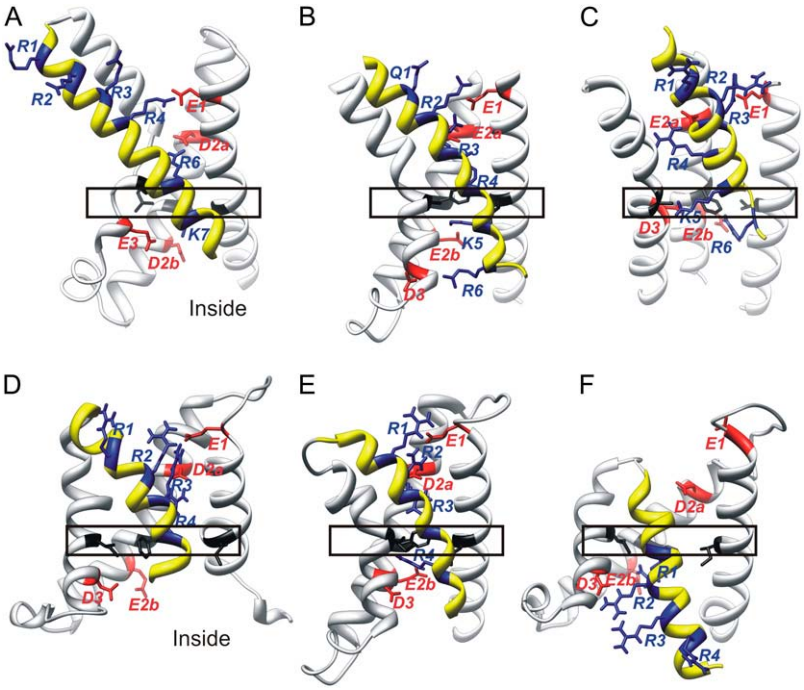

FIGURE 1 Ribbon representations of VSDs: S1–S3 have white backbones, and S4 has a yellow backbone. Generic residues are shown and named as in Fig. 2. Negatively charged generic residues of S1, S2, and S3 are colored red, positively charged generic residues of S4 are colored blue, and hydrophobic transition barrier residues of S1, S2, and S3 are colored black and enclosed in rectangles. The VSDs are oriented with the *y*-axis orthogonal to the plane of the membrane and parallel to the axis of the pore, with the extracellular portion at the top. (*A*) Crystal structure of an isolated VSD from KvAP (5). (*B*) Crystal structure of VSD from Kv1.2/2.1 chimera (6). (*C*) Model of VSD of a *Shaker* channel that preceded crystal structures (7). (*D*) The $Open_2$ model of NaChBac. (*E*) $Open_1$ model of NaChBac. (*F*) $Closed_{0a}$ model of NaChB.

membrane during gating, most of which is carried by the first four arginines (*R1–R4*) of S4 (10–12). We thus proposed that S4 should move ~3 helical screw steps, i.e., rotate ~180° and translate ~13.5 Å, for the four S4 segments to produce the measured gating charge (7). This movement positions the first arginine, *R1*, of the resting conformation in the location occupied by the fourth arginine, *R4*, of the open conformation.

Recently determined crystal structures of a Kv1.2/Kv2.1 chimera and MlotiK channels reveal that substantial portions of S4 may adopt a 3_{10} helical structure, and that the regions of S4 that form an α- or 3_{10} helix may differ in open and closed conformations. These findings suggest that the motions of S4 may have additional elastic properties that allow it to stretch out ($\alpha \rightarrow 3_{10}$ transition) or spring back ($3_{10} \rightarrow \alpha$ transition) in response to voltage changes. The new elastic helical screw models presented here explore the implications of these types of secondary-structure changes on activation gating of NaChBac. We also compare these more dynamic models to models in which S4 moves as a rigid α-helix.

Most voltage-gated channels, including NaChBac (13), appear to have multiple closed conformations. Although we developed several models of closed NaChBac channels, our $Closed_1$, $Closed_2$, and $Closed_3$ transition models should not be interpreted as representing specific low-energy conformations. Rather, they are presented simply to demonstrate the feasibility of general pathways predicted by the rigid and elastic helical screw models, and to illustrate our rationale for developing models of closed conformations. Our $Closed_0$ models are intended to indicate the innermost position of S4 when the membrane is hyperpolarized. We avoid calling these resting conformation models, because there may be a thermodynamic equilibrium among several conformations at resting voltages.

The NaChBac and K_v channels also inactivate at positive voltages, and many of the structural data used to model ''open'' conformations likely come from inactivated conformations. We have not attempted to model the poorly understood inactivation process. Here, we labeled the models of depolarized conformations as $Open_1$ and $Open_2$, to emphasize that we are modeling the activation and not the inactivation process. However, one or both of these models may correspond more closely to an inactivated conformation.

METHODS

Methods of developing the models and performing MD simulations are described in our accompanying study. The transmembrane electrostatic fields were calculated by methods similar to those previously described (14,15). Specifically, the PBEQ module of the CHARMM software package was used to solve the Poisson-Boltzmann equation, using finite differences. The system consisted of the full, tetrameric channel protein embedded in a membrane of explicit lipid molecules. The coordinates are from the snapshot at the end of the equilibration stage of MD simulations. The regions occupied by aqueous solvent were assigned a macroscopic dielectric constant of 80, and those of the protein and membrane were assigned a dielectric constant of 2. Ionic strength was set at 150 mM. The cubic grid consisted of 170 elements along each edge, with a resolution of 1.0 Å/element. According to the logistics of the PBEQ module, an arbitrary transmembrane potential of 1.0 V was applied across a 2.5-nm, low-dielectric (i.e., a dielectric constant of 2) slab, superimposed on the hydrophobic core of the explicit membrane. The specific width of this slab was chosen by fitting the distance between the two not-completely-flat, lipid headgroup/alkyl chain interfaces of the membrane. In addition, a high-dielectric (i.e., a dielectric constant of 80) cylinder of 10-nm diameter was centered on the pore, perpendicular to the membrane plane. This provided the model with the effects of waters that may fit in the pore

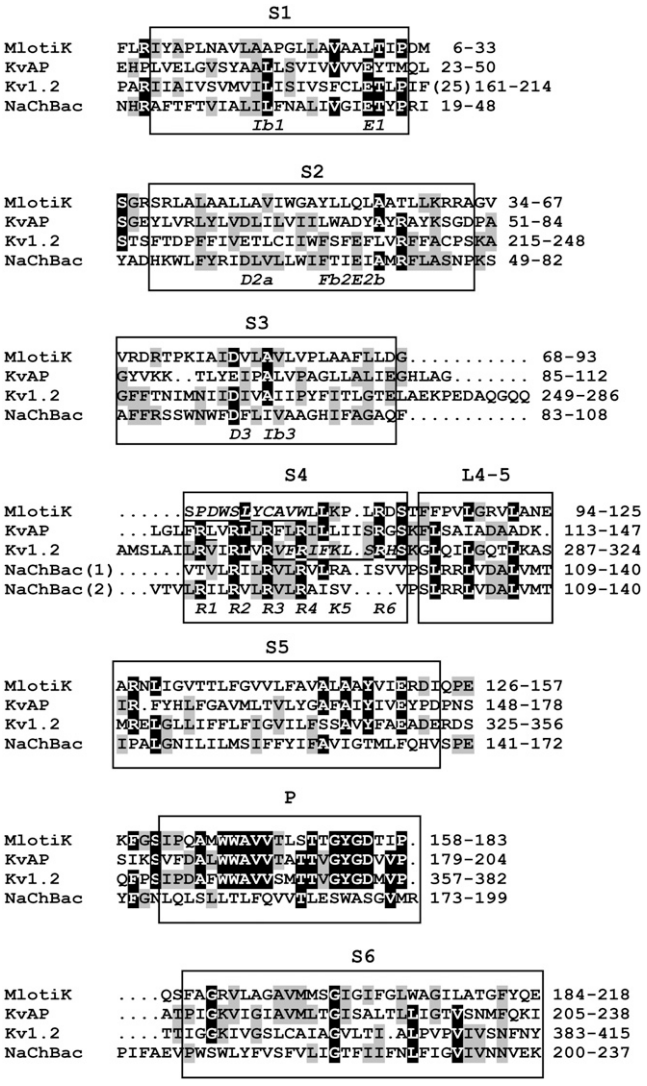

FIGURE 2 Multisequence alignment of transmembrane region of MlotiK, NaChBac, Kv1.2, and KvAP sequences. Residues for which at least three residues are identical among the four sequences have black backgrounds, and those with two identities have gray backgrounds. Two alignments are presented for S4 of NaChBac, as explained in the text. Generic names for some crucial residues within the VSD are indicated in italics below the NaChBac sequence. ''(25)'' at the end of S1 in Kv1.2 indicates an insertion of 25 additional residues.

and the cavities of the protein and lipid headgroups on the intracellular and extracellular sides of the membrane. Finally, all protein and lipid atom charges were neutralized, to calculate only the potential attributable to the applied transmembrane voltage.

The resultant electrostatic fields were used for calculating gating charges between different conformational states of the protein. Specifically, for each system, the contribution of each atom to the electrostatic free energy was calculated by multiplying its charge by the potential at its location. Taking the difference in these values between open and closed states of the protein, summing over all atoms, and dividing by the applied transmembrane potential (1.0 V in this case) result in the amount of charge that transverses the transmembrane field because of the conformational change, which defines the gating charge.

RESULTS

Alignments

Alignments used in developing the models are given in Fig. 2. The alignment between NaChBac and K_v sequences is unambiguous for S1, S2, and S3 segments because numerous key residues, including rare transmembrane charged residues, are conserved both within and between both superfamilies. Aligning S4 is problematic because the highly conserved residues are the arginines, and the tripeptide repeating pattern, $(RXX)_n$, is longer in K_v channels than in NaChBac. In homology modeling, it is important to relate sequence alignments to structural alignments. To illustrate this point, we compared the VSD crystal structures of the Kv1.2/2.1 chimera (6) with those of the isolated KvAP (5). Fig. 2 gives the alignment generally considered to be best, in which *R1*, *R2*, *R3*, and *R4* of both sequences align. However, Fig. 1, *A* and *B*, indicates that *R3*, *R4*, *R5*, *R6*, and *K7* of the KvAP crystal structure are positioned near the locations occupied by *Q1*, *R2*, *R3*, *R4*, and *K5*, respectively, of the Kv1.2/2.1 crystal structure. Using the terminology of the helical screw model, one could say either that S4 of the KvAP crystal structure is positioned two helical screw steps farther out than in Kv1.2, or that the KvAP sequence should be shifted by six positions to the left, to agree with the structural alignment. As an additional complicating factor, the magnitude of S4 movement may differ among channels. For example, we suggest that S4 may move ~1 helical screw step farther in NaChBac than in *Shaker* or Kv1.2, and that S4 of KvAP may move ~1 helical screw step farther than in NaChBac. Thus, the first alignment of S4 in Fig. 2 for NaChBac and Kv1.2 may be appropriate for the resting conformation, whereas the second may be appropriate for the open conformation.

The MlotiK channel is gated by cyclic nucleotides instead of voltage (16). This likely explains why the sequence of its S1–S4 domain is distant from those of NaChBac and Kv1.2, and its S4 has no positively charged residues that align with *R1–R4*. Nonetheless, its sequence can be aligned unambiguously with that of Kv1.2 by comparing the two crystal structures. This structure-based alignment is strengthened insofar as the alignment between NaChBac and MlotiK, inferred from our alignment of NaChBac with Kv1.2, has no insertions or deletions (indels) from the beginning of S1 through the P segment.

The S3-S4 loop region tends to be poorly conserved within families of voltage-gated channels, frequently contains residues such as proline, glycine, serine, asparagine, and aspartate that have a low propensity for helical secondary structure, and often have indels (personal observations). This is the case within the alignment of NaChBac homologues. The S3-S4 loop is formed by residues 106–108 (AQF) for our open models, and by residues 103–105 (FAG) for our $Closed_0$ models. Many NaChBac homologues have proline at positions aligning with F103 and F108, have a one-residue deletion between these residues, and typically have other

residues with a high propensity for coil conformations within this region. For example, the FAGAQF sequence of NaChBac aligns with the PSSG-P and PSND-S sequences of some homologues.

Open conformations of the VSD

Minimizing the number of indels simplifies homology modeling. The first alignment of NaChBac with Kv1.2 for S4 in Fig. 2 has no indels from the beginning of S4 through the end of the P helix. Our $Open_1$ model is based on this alignment. Although the Kv1.2 crystal structure (17) was used initially in developing our models, the model of the VSD in Fig. 1 *E* was developed from the recently determined Kv1.2/2.1 chimera structure (6), which has a higher resolution that defines specific residues in S1 and S3 not identified in the Kv1.2 structure, and provides coordinates for all side chains and connecting loops. When modeled after the Kv1.2/2.1 chimera, aromatic side chains F84 and F85 of the S2-S3 loop reside in the transmembrane region near the inner headgroup region, where they interact with one another and with other aromatic side chains F75, W91, and F94. This S2-S3 structure was chosen for both open and closed models over models developed from the MlotiK crystal, because aromatic-aromatic interactions are energetically favorable (18), and aromatic side chains occur frequently at membrane surfaces (19). The S1-S2 and S3-S4 loops are shorter in NaChBac than in the Kv1.2/2.1 crystal, and are the most ambiguous parts of the model because they were not modeled from a crystal template.

Fig. 1, *B* and *E*, illustrates common features of the $Open_1$ model of NaChBac and the Kv1.2/2.1 chimera for the VSD. The $Open_1$ model satisfies our evolutionary criteria quite well, e.g., most of the poorly conserved hydrophobic residues of S1–S3 segments are on the external surfaces where they interact with lipids, and the core of the VSD is composed of highly conserved residues, with salt bridges forming between negatively charged residues of S1–S3 and positively charged residues of S4. Most of the salt bridges are conserved in both models. Charged residues can be classified as outer charges (*E1, E2a, R1, R2*, and *R3*) and inner charges (*E2b, D3*, and *R4*). Studies of *Shaker* K^+ channels suggest that much of the transmembrane voltage change occurs across a relatively short region in the VSD, and that most of the contribution of a positively charged residue of S4 to the gating current occurs as it crosses this transition barrier (20). The outer and inner charged clusters are separated by a highly conserved hydrophobic region formed by residues on S1 (*Ib1*), S2 (*Fb2*), and S3 (*Ib3*) in the NaChBac model. These residues (Fig. 1, *black*) likely comprise much of the postulated transition barrier.

If the $Open_1$ model is correct and forms the only open conformation, then *R4* should not contribute substantially to the gating charge, because it is part of the inner cluster and would not cross the transition barrier during gating. This conclusion seems inconsistent with the large gating charge ($e_o \sim 16$) that was calculated for NaChBac (13). This observation led us to develop models in which S4 is positioned one or two helical screw steps farther outward. Models with S4 positioned two helical screw steps farther outward (similar to the position of S4 in the KvAP crystal structure) were not stable during MD simulations, i.e., after a few cycles of 6-ns simulations followed by modeling to restore fourfold symmetry, the S4 segments moved inward, to the vicinity of models constructed with S4 positioned only one helical screw step outward. In contrast, models with S4 moved only one helical screw step outward (i.e., consistent with alignment 2 of Fig. 2) converged after a few simulations to structures that were even more stable during final simulations than was the $Open_1$ model. The VSD of the $Open_2$ model is shown in Fig. 1 *D*. The major advantage of the $Open_2$ model is that the charged groups of all four arginine side chains of S4 are exterior to the transition barrier, and thus could all contribute to the gating charge. The *E2bK* and *D3K* mutations in the inner cluster were shown to shift the voltage-current (V-I) curve to the left (21), indicating that mutations of the inner charges stabilize open, relative to resting conformations. These results are more consistent with the $Open_2$ model, because none of the positively charged side chains of S4 are near *E2b* or *D3* in the $Open_2$ model. In contrast, *R4* binds to *E2b* in the $Open_1$ model, and *R1* and *R2* bind to *E2b* and *D3* in the $Closed_0$ models (described below).

Differences between the final $Open_1$ and $Open_2$ models involve more complexity than the position of S4. With respect to one another, S1, S2, S3, and S4 all shifted, and the inner-pore region of the pore domain (PD) expanded. Despite differences between the $Open_2$ model and the Kv1.2/Kv2.1 structure, the salt-bridge interactions are preserved, i.e., *R2* binds to *E1*, *R3* to *E1* and *D2a*, and *R4* to *D2a* in the model, as they do in the Kv1.2/2.1 crystal structure.

A Poisson-Boltzmann calculation of the gating charge (14) predicted e_o values of 10.8 and 15.4 for transitions from the $Closed_{0a}$ model described below to $Open_1$ and $Open_2$ models, respectively. These calculations support our hypothesis that the $Open_2$ model is a better representation of the open conformation. Shapes of electric fields within these models, based on these calculations, are illustrated in Supplementary Fig. S1. These calculations indicate that the electric field is quite distorted within the pore of the PD, especially in the open models, but it is not distorted much within the VSD of either the closed or open models. This lack of distortion within the VSD is probably attributable to the narrowness of the crevasses in these models.

Consistency with LRET data

Richardson et al. (22) used luminescence resonance energy transfer (LRET) spectroscopy to measure distances between identical residues on adjacent NaChBac subunits. A number of different fluorescent probes were attached to cysteines introduced one at a time at 21 positions: nine positions

throughout S4, the first four positions in L4–5, and seven positions in other segments. Distances calculated from these studies are compared in Table 1 with the distances between β carbons of the corresponding residues for the $Open_2$, $Open_1$, and Kv1.2/2.1 crystal structure. Distances that are within 5 Å of the LRET distances are indicated in bold, and the distance for the three structures at each location that is nearest the LRET distance is underlined. The $Open_2$ model is more consistent than $Open_1$ with the LRET data. Its distances are better for 15 positions (Table 1, *underlined*), and are within 5 Å at 11 positions (Table 1, *bold*). The best agreement occurs for the S4 and L4–5 segments from residues 109–128. Nine of 11 positions are within 5 Å for the $Open_2$ model. Data from other segments are less consistent: only 3 of 10 positions are within 5 Å. The LRET distances for three residues on S1 are slightly less than those for two residues on S6. This is surprising, because the VSD is peripheral to the PD in the known structures, and the distances calculated for the analogous positions on the Kv1.2/2.1 structure are substantially greater (about twice as long) for S2 than for S6 (Table 1). The greatest discrepancy occurs at residue 25, located at the beginning of S1. The analogous position in the MlotiK structure precedes the helical region of S1, which begins at its L13 residue. In the $Open_2$ model, the S1 helix was initiated at residue F27, so that the discrepancy with the LRET data for residue 25 could be reduced. However, even this adjustment was insufficient to eliminate the apparent deviation. Residues 40 and 43 at the end of S1 are nearer the axis of the pore (which is proportional to the residue-residue distance for adjacent subunits), and residue 231 near the end of S6 is farther from the axis in the $Open_1$ model. Thus, the shifts in the $Open_2$ model from the $Open_1$ model and Kv1.2 template reduce the discrepancies for S1, L4–5, and S6 residues, but do not eliminate them.

TABLE 1 Distances between residues and their counterparts on an adjacent subunit calculated from LRET studies (22), and measured in models and the Kv1.2/2.1 chimera

		Distance between C_β of adjacent subunits (Å)			
Segment	Residue	LRET	$Open_2$	$Open_1$	K_v crystal
S1	25	30.0	47.7	56.7	58.8
	40	28.3	39.5	40.5	42.3
	43	28.0	37.6	39.8	43.2
S3	88	49.4	**50.7**	**49.8**	42.2
	98	47.8	64.2	57.0	**53.2**
S4	109	54.0	**56.2**	**52.1**	**50.6**
	112	47.6	**48.9**	**52.1**	**49.1**
	114	49.1	**52.7**	43.1	38.8
	118	54.9	**51.5**	44.6	40.8
	120	43.2	**41.0**	**38.3**	36.5
	123	44.5	**42.0**	39.4	39.1
	124	53.0	42.6	44.2	37.7
	125	48.6	**49.6**	**44.3**	**44.9**
	126	40.7	49.2	**38.3**	**43.3**
L4-5	127	43.2	**42.6**	36.8	35.8
	128	42.3	**42.4**	36.7	34.2
	129	50.3	36.4	30.5	29.6
	130	48.3	39.1	32.5	32.9
Pore	190	9.9	**14.3**	**12.1**	**5.1**
S6	208	29.9	**25.1**	24.6	**25.9**
	231	31.4	21.5	15.8	16.9

Bold indicates that the LRET distance is within 5 Å of the distance in the models. The structural distance in best agreement with the LRET distance is underlined.

Models of resting and transition states

Once our models of open conformations were completed, we developed models of closed channels. We used two approaches. Our first approach was to begin with the VSD in the $Open_1$ conformation but interacting with a closed PD, modeled using the KcsA crystal structure as the initial template. Then we S4 moved inwardly by three successive helical screw steps predicted by the helical screw model, to generate the $Closed_0$ model. We call this the ''rigid helical screw'' mechanism, because S4 moves as a rigid body and maintains a predominantly α-helical conformation throughout the transitions. Two transition models for this mechanism are illustrated in Fig. 3 *A*. In the $Closed_{2a}$ model, where the subscript 2 indicates that two S4 arginines are above the transition barrier, S4 has moved inwardly from the putative $Open_1$ conformation by ~1 helical screw step. Each of the four arginines forms a salt bridge with at least one of the four negatively charged residues on S1–S4. This model illustrates that the negative charges are well-positioned to interact with positively charged residues of S4 if it moves in this manner. This point was made previously for transition-state models of KvAP (9). In the next model ($Closed_{1a}$, second from left in Fig. 3 *A*), S4 has moved inwardly two helical screw steps relative to the $Open_1$ model. Although this model has one fewer salt bridges than the previous step, the amount of helical secondary structure has increased because of the shortening of the connector between the S4 and L4–5 helices. The $Closed_{0a}$ model was developed by moving S4 inward by yet another helical screw step. Multiple MD simulations, with readjustments between simulations that restored four-fold symmetry, were performed to obtain the final version of this model. In this model, all four of the arginines of S4 are interior to the transition barrier, and *R1* and *R2* bind to *E2b* and *D3*.

Our second approach was to use the recently determined MlotiK crystal structure to explore an alternative, more dynamic mechanism of S4 movement. We will call this the elastic helical screw mechanism because, in addition to the rotation and translation motions, portions of the S4 helix may stretch out ($\alpha \rightarrow 3_{10}$ transition) or spring back ($3_{10} \rightarrow \alpha$ transition) in response to voltage changes. This hypothesis is based on a comparison of the MlotiK and Kv1.2/2.1 crystal structures. The portion of the Kv1.2/2.1 structure that aligns (alignment 1) with NaChBac residues 109–116 of the N-terminus of S4 has an α-helical structure. The italicized

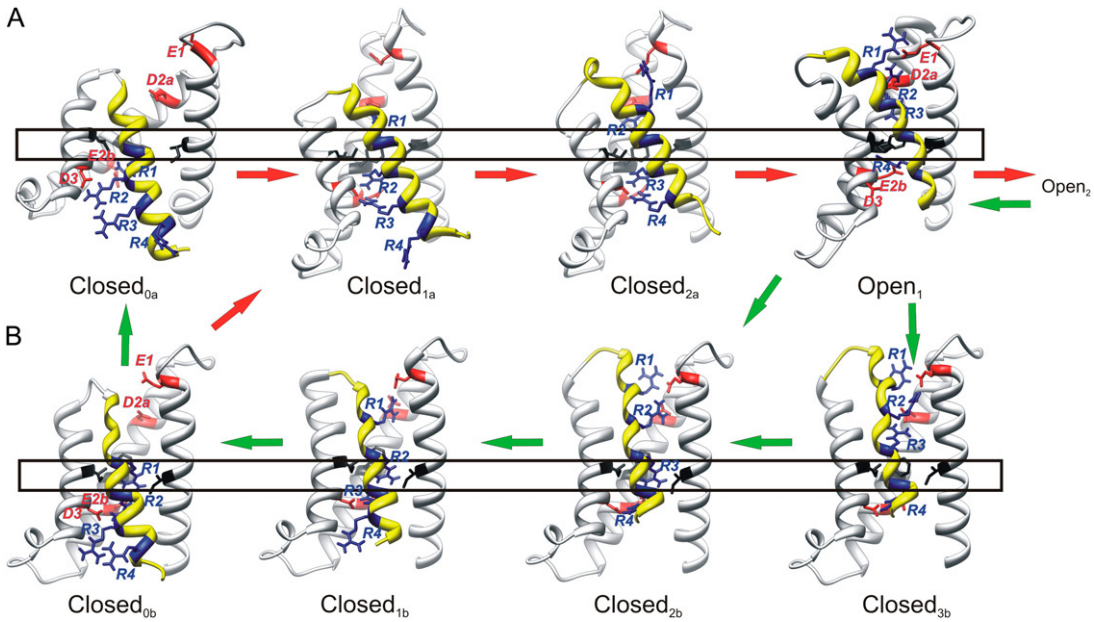

FIGURE 3 Models of NaChBac VSDs with S4 in innermost and transition positions. Coloring, orientation, and labels are the same as in Fig. 1. Closed models are numbered according to the number of S4 arginine guanidium groups located above the transition barrier, as indicated by rectangles. Arrows indicate plausible pathways for activation at positive voltages (*red*), and deactivation at negative voltages (*green*), if voltage-dependent changes in secondary structure occur more rapidly than the transitions between the $Closed_0$ and $Closed_1$ and $Closed_2$ models. (*A*) A rigid helical screw mechanism, in which S4 maintains a predominately α-helical conformation as it transitions from hyperpolarized closed to $Open_1$ conformations. (*B*) An elastic helical screw mechanism, in which the N-terminus portion of S4 adopts a 3_{10} helical secondary structure in closed conformations. The MlotiK crystal structure was used as a template for the S2, S3b, and S4 portions of $Closed_{2b}$ and $Closed_{3b}$ models. The primary difference between the $Closed_{2b}$ and $Closed_{3b}$ models is the conformation of the *R3* side chain.

and underlined portion in Fig. 2 that aligns with residue NaChBac residues 117–126 of the C-terminus of S4 forms a 3_{10} helix. In contrast, the italicized and underlined portion of MlotiK in Fig. 2 that aligns with NaChBac residues 110–119 of the N-terminus of S4 forms a 3_{10} helix, and the portion that aligns with NaChBac residues 120–126 of the C-terminus of S4 forms an α-helix. Thus, if MlotiK is used as a template for a closed conformation of NaChBac, then the conformational change from the $Open_1$ Kv1.2-like conformation to a MlotiK-like closed conformation involves a substantial change in the secondary structure of S4 (Fig. 3 *B*). The transition models called $Closed_{2b}$ and $Closed_{3b}$ of the NaChBac VSD in Fig. 3 *B* were developed by modeling the S2, S3, and S4 portion after the MlotiK crystal structure. The structures of S1, the S1-S2 loop, and the S2-S3 loop of the $Open_1$ model were retained because the sequence of the VSD of NaChBac is more like that of Kv1.2 used to model these segments, and we wanted to minimize the conformational changes within the VSD during gating. We call these models $Closed_{2b}$ and $Closed_{3b}$ because the interactions of the charged residues of these models are similar to those in the $Closed_{2a}$ and $Open_1$ models of Fig. 3 *A*, despite the differences in secondary structure. This similarity is possible because the arginine side chains are long and relatively flexible.

The changes in secondary structure for a transition from the $Open_1$ model to the $Closed_{2b}$ and $Closed_{3b}$ models have the following consequences: 1), the N-terminus of S4 moves outwardly ~4 Å relative to the plane of the membrane, rotates ~45° about the axis of the helix, and moves nearer the core of the VSD; 2), all four arginine side chains now extend into the negatively charged core of the VSD, where they form salt bridges with negatively charged side chains within S1-S3; and 3), the midregion experiences little rotation, and only slight inward translation (2–3 Å). This translation moves the positively charged group of the *R3* side chain from a position above the transition barrier, where it binds to *E2a* in the $Open_1$ model, to a position within the transition barrier that is midway between *D2a* and *E2b*. In the MlotiK crystal structure, the β carbon of the MlotiK residue that aligns with *R3* is 7.5 Å below the β carbon of the residue that aligns with *D2a*, and 7.4 Å above the β carbon of the residue that aligns with *E2b*. The *R3* and the two residues that precede it retain a 3_{10} conformation in both models. The marked differences between the motions of the N-terminus and midregion are attributable primarily to secondary-structure transition. The α-3_{10} transition elongates the helix (because the rise per residue increases from ~1.5 Å to ~2.0 Å), and rotates one end of the helix relative to the other (because the rotation per residue about the axis changes from ~100° to ~120°). The C-terminus of S4 also moves differently from the midregion, because of the conversion of residues 120–126 from 3_{10} to α in the transition from $Open_1$ to $Closed_{2b}$. This putative

shortening of the C-terminus end of S4 during deactivation reduces its extension into the cytoplasm and increases the cross-sectional area, which may affect the position of L4–5 and its interaction with S6.

The location of the side chain of *R3* in this model is especially interesting because it suggests how the bulky and charged arginine chains can traverse the hydrophobic transition barrier, and how side-chain conformational changes may contribute to the gating current. In the $Closed_{2b}$ model of Fig. 3 *B*, the *R3* side chain extends downward between hydrophobic side chains *Ib1* and *Fb2* of the transition barrier, allowing its guanidium group to form salt bridges with the *E2b* side chain (Fig. 4). The interaction between the planar surface of the guanidium group of *R3* with π-electrons of the aromatic ring of *Fb2* and a hydrogen bond formed to the side chain of N36 of S1 may help lower the energy. This configuration should be stabilized by negative transmembrane voltage. In the $Closed_{3b}$ model, the *R3* side chain extends outwardly to salt-bridge to the side chain of *D2a*, while maintaining a hydrogen bond to N36 (Fig. 4 *B*). This configuration should be favored by positive voltages. Thus, voltage-dependent conformational changes of the charged side chains may contribute to a fast component of the gating current. The backbone of S4 in the $Closed_{3b}$ model is shifted outwardly by ~1 Å relative to that of the $Closed_{2b}$ model, to facilitate formation of a salt bridge of *R3* to *D2a*. The backbone positions of the $Closed_{2b}$ and $Closed_{3b}$ models flank the analogous position of S4 in the MlotiK crystal structure. Additional voltage-dependency of the $Closed_{2b}$ to $Open_1$ transition could arise from a shift of the electric field caused by a reduction of the water-accessible volume inside the outer VSD crevasse.

This elastic transition between the $Open_1$ and $Closed_{2b}$ models alone is insufficient to account for all of the large gating current of NaChBac, or to explain the results of numerous studies on the position of the resting S4 in other channels. It could, however, facilitate additional transmembrane movements. For example, the conversion of the N-terminus portion to a 3_{10} helix gives the S4 helix rather large, smooth groves between the three columns of side chains, and reduces the cross-sectional area of the helix. These effects may allow S4 to slide inwardly toward the cytoplasm during deactivation (or outwardly during activation) past large side chains (such as *Fb2* of the transition barrier or Y156 of S5) in a simple manner that involves no substantial rotation. For channels such as NaChBac that have short S3–S4 linkers, the elongation and reduction of the tilt of S4 caused by the presence of an N-terminus 3_{10} helix region may allow the charged region of S4 to move farther inward without pulling the polar S3 C-terminus, S4 N-terminus, and S3–S4 linker far into the transmembrane region. As S4 moves inwardly during deactivation past the transition barrier, the inner portion of S4 may transition to an α-helical conformation. The additional movements that precede or follow the putative elastic transition can be modeled in steps similar to the helical screw

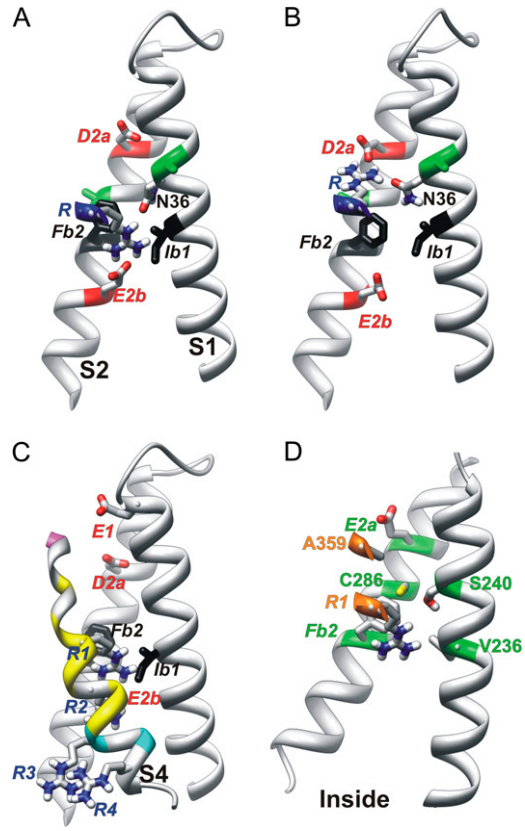

FIGURE 4 Side view of S1, S2, and portions of S4 of $Closed_b$ models. Side chains of N36, *D2a*, *E2b*, and an S4 arginine are colored by atomic element (*red*, oxygen; *blue*, nitrogen; *white*, hydrogen; *gray*, carbon; and *yellow*, sulfur). Transition barrier residues are black. (*A* and *B*) An S4 arginine is oriented (*A*) inwardly for negative voltages, where it salt-bridges to the *E2b* group, and (*B*) outwardly for positive voltages, where it salt-bridges to the *D2a* group. Although this representation was generated from $Closed_{2b}$ and $Closed_{3b}$ models in which the arginine is *R3*, it could be used for $Closed_b$ models favored at more negative voltages, in which the S4 arginine would be *R1* or *R2*. Green positions on S1 and S2 (*A* and *B*) indicate residues analogous to *Shaker* I241C and I287C, which can cross-link with the *R1C* residue at negative voltages in *Shaker* channels (24). (*C*) $Closed_{0b}$ model, in which S4 residues are colored according to accessibility to [2-(trimethylammonium)ethyl]-methanethiosulfonatein at negative voltages of introduced cysteines at analogous positions in *Shaker* channels (25), using alignment 2. Magenta indicates accessibility from the outside, cyan accessibility from the inside, and yellow inaccessibility from either side. (*D*) $Closed_{0b}$ model of the *Shaker* channel illustrates residue positions where mutations have a strong, apparently steric effect on Ω currents (27).

steps in which the *n*th residue moves to the position occupied by the $(n \pm 3)$th residue before the step. This approach was used to develop the $Closed_{1b}$ and $Closed_{0b}$ models Fig. 3 *B*. The $Closed_{0b}$ model is an alternative model for the most inward conformation of S4. However, we do not favor this model because it was substantially less stable during MD simulations than was the $Closed_{0a}$ model, and the gating charge calculated for a transition from the $Closed_{0b}$ to $Open_2$ models was ~2 e less than from the $Closed_{0a}$ model.

The rigid and elastic helical screw mechanisms described above have several features in common. In both, positively

charged S4 residues located in the central portion of the transmembrane region are positioned in the core of the VSD, where they can interact with negatively charged residues of S2 and S3. Although estimates of the energy required to translocate arginines across a lipid bilayer by alternative routes in which they are exposed exclusively to lipid alkyl chains vary substantially (23), there is no dispute that a pathway in which the S4 arginines interact with negatively charged groups and water within clefts will be electrostatically more favorable. In our $Closed_0$ models, the charged groups of all four arginines of S4 are interior to the transition barrier. This feature is consistent with the magnitude of the gating charge in NaChBac (13), which, if attributable solely to the movement of the charges of S4, suggests that all four S4 arginines traverse most of the transmembrane field during gating. A *D2aK* charge-reversal mutation in NaChBac shifts the activation V-I curve to the right dramatically, indicating that reversing the charge of this outer residue stabilizes resting conformations relative to the open conformation (21). This result also supports models in which positively charged side chains bind to *D2a* in the open but not resting conformations.

Our current working hypothesis is that the voltage-dependent movement of S4 is likely to be a highly dynamic process. For example, if S4 is a flexible and elastic structure, it may move through many different pathways during multiple gating events, some of which could be similar to the elastic screw mechanism. Others could be more like the rigid screw trajectory, and others could be somewhere between. It is also possible that S4 moves differently during activation at positive voltages than it does during deactivation at negative voltages. For example, if side-chain and elastic secondary-structure conformational changes occur more rapidly than do the larger translocations and rotations, then during activation, the pathway could be similar to that indicated by the red arrows in Fig. 3, whereas the deactivation pathway could be similar to that indicated by the green arrows. It is also possible that S4 moves differently in different channels, e.g., the 3_{10} structure may be more important in channels that have short S4 segments with short linkers to S3 and L4–5, and may not be present in KvAP, for which no 3_{10} structure within S4 has been observed in crystal structures. Rigorous computational analyses of these types of conformational transitions are beyond the scope of our study, and would best be performed using experimentally determined crystal structures of the same channel in both open and resting conformations.

Consistencies of closed models with experimental studies of *Shaker* channels

Shaker is the most studied voltage-gated channel. It is thus important to determine whether models of other voltage-gated channels are consistent with results obtained from *Shaker*. Here we describe how the $Closed_0$ and $Closed_1$ models are consistent with results of numerous experiments.

The most compelling evidence for a location of *R1* of *Shaker* within the transition barrier region for resting conformations was provided by Ahern and Horn (20). They found that positively charged adducts, attached to a cysteine introduced into the *R1* position, contribute a full charge per subunit to the gating charge, e_o, if the tether between the sulfhydryl and charged group is short. However, the charge contribution is reduced and becomes negligible as the length of the tether is increased from three to six carbons. An explanation suggested by our NaChBac models is that *R1* is positioned within the transition barrier at negative voltages, and that the short adducts can extend inwardly through the transition barrier so that their positively charged moiety binds to *E2b* of the inner charged cluster (similar to arginine in Fig. 4 *A*). If so, then the adduct would contribute ~1 charge per subunit to e_o, because the charge would move across the transition barrier to the outer surface when the channel activates. However, the longer, bulkier adducts may not be able make the transition to the inner cluster because of steric interactions within the highly conserved residues of the transition barrier and inner cluster. This would force the long adducts to extend outwardly and interact with negative charges of the outer cluster, even at negative voltages (similar to arginine in Fig. 4 *B*). Thus, when the channel activates, the longer adducts would contribute little if any gating charge, because their charged moiety is near the outer surface at all voltages. Our calculation that the electric field is not narrowly focused across the transition barrier (see the Supplementary Material, Fig. S1) is inconsistent with the hypothesis of Ahern and Horn (20), that most of the voltage drop occurs through a very short distance approximated by the differences between the lengths of the short and long tethers. However, in our explanation, differences in the conformations of the short and long tethers, accompanied by possible differences in the inward-most position of S4 with long and short tethers, should make the distances at negative voltages between the locations of the charges at the ends of the tethers much greater than the differences between the lengths of the tethers, e.g., the length of the arginine side chain does not change from Fig. 4, *A* to *B*, but the transmembrane location of its charged group does.

Campos et al. (24) found that when *R1* and either I241 on S1 or I287 on S2 are replaced with cysteine in *Shaker* channels, disulfide and Cd^{2+} bridges form at negative voltages. The NaChBac residues that align with I241 and I287 are colored green in Fig. 4, *A* and *B*. These residues are slightly above *R1* in the $Closed_{0b}$ model in Fig. 3 *B* (similar to the position of the arginine in Fig. 4 *A*), and are below *R1* in the $Closed_{1b}$ model (not shown). The *R1C* residue may be positioned somewhat higher (more outward) at negative voltages than in native channels, because there is no electrostatic force to draw *R1C* past the transition barrier in these mutants. Thus, these results are also consistent with a location of *R1* within, or just above, the transition barrier region at negative voltages.

These models were also consistent with the results of studies regarding voltage dependencies of the accessibilities to charged sulfhydryl reagents from each side of the membrane of cysteines introduced throughout S4. The S4 in the $Closed_{0b}$ model is colored in Fig. 4 *C* according to the accessibilities to [2-(trimethylammonium)ethyl]-methanethiosulfonatein of cysteines introduced into S4 of *Shaker* at negative voltages (25). Alignment 2 in Fig. 2 was used to identify NaChBac residues analogous to the mutated *Shaker* residues. The magenta residue was accessible from the outside, yellow residues were inaccessible from either side, and cyan residues were accessible from the inside in full-length *Shaker* channels. The inaccessible residues (yellow) were located near the middle of the membrane, and spanned the transition barrier region.

Results of studies of Ω currents are also consistent with a $Closed_{0b}$-like model for hyperpolarized *Shaker* channels. Tombola et al. (26) found that when *R1* is mutated to a small uncharged residue, current flows through the VSD at hyperpolarized voltages. Tombola et al. (27) analyzed effects on these Ω currents of mutations in the outer portions of S1, S2, S4, S5, and S6 segments. The strongest, apparently steric effects were found for residues on S1 (V236 and S240) and S2 (E283, C286, and F290) that contribute to the core of the VSD, and A359 on S4, which precedes *R1* by three residues. Fig. 4 *D* illustrates A359 and the *R1* residues in the core of the VSD in close proximity to the Ω current-sensitive residues of S1 and S2, in a model of *Shaker* developed from the $Closed_{0b}$ model of NaChBac.

The results from *Shaker* channels least consistent with the models presented here are based on LRET measurements of distances between probes attached to a pore-blocking scorpion toxin and residues 361 (immediately preceding *R1*) and 365 (corresponding to *R2*) (28). The outward translocation of S4 during activation gating was estimated to be ~2 Å in these studies, i.e., much less than in the $Closed_0$ or $Closed_1$ to $Open_1$ models presented here, or models proposed by others (6–15). The simplest explanation for these results is that a thermodynamic equilibrium exists among numerous closed conformations, and these results reflect closed conformations in which S4 is positioned near its location in the open conformation. For example, based on our NaChBac models, residues analogous to *Shaker* 361 and 365 move 3.4 Å and 6.7 Å outward for the transition from the $Closed_{1b}$ to $Open_1$ model, respectively, and 3.4 Å *inward* and 1.1 Å outward for the transition from the $Closed_{2b}$ to $Open_1$ model, respectively. A bias toward more outward closed conformations could be attributed to two effects. First, the signal from LRET studies is inversely proportional to the sixth power of the distance between probes, and will be dominated by conformations for which the distance is shortest. If different closed conformations similar to those in Fig. 3 are all present simultaneously, then the distance measurement between a probe attached to the N-terminus of S4 and another probe attached to a surface-bound toxin (28) will be skewed toward the $Closed_2$ and $Closed_3$ type conformations, for which distances between probes are shorter. Moreover, the attachment of large LRET probes to positions near the N-terminus of S4 may skew the distribution of closed conformations to favor the more outward conformations, e.g., attachment of a large adduct at the *R2* position may inhibit translocation of the *R2* position beyond the transition barrier, and thus inhibit formation of $Closed_0$ and $Closed_1$ types of conformations. Furthermore, the constricted space within the outer crevasse of the VSD may cause the relatively large LRET probes on S4 to orient preferentially toward the outer surface, as suggested above for long charged adducts at the *R1* position that do not contribute to the gating charge.

Interactions between the VSD and PD

According to one of our modeling criteria, residues conserved on the surface of one domain tend to interact with residues also conserved on the surface of the interacting domain. This criterion is not well-satisfied by models in which the VSD docks on the PD in the position observed in the Kv1.2 and Kv1.2/2.1 crystal structures. Examination of differences between conservation patterns of residues that in our models are on the external surfaces of each transmembrane domain suggest that the domain interactions differ slightly in the two proteins. For example, in our NaChBac model, the highly conserved G41 (on the outer surface S1) and Y156 (on the outer surface S5) align with poorly conserved hydrophobic residues in Kv channels. We thus explored alternative packing between the two domains. In the final models that we favor for the $Open_1$ conformation, the VSD is rotated slightly from its location in the Kv1.2 crystal (Fig. 5). The adjustment positions the two domains in a manner more like that of the MlotiK crystal structure. Numerous interactions of conserved residues on the outer surface of S5 with conserved residues on the outer surfaces of S1 and S4 of the open conformation are illustrated in Fig. 6 *A*. The Y156 side chain of S5 extends between S1 and S4, where its hydroxyl group binds to conserved N36 and *R3* (in $Open_1$) or *R4* (in $Open_2$) side chains, whereas its aromatic ring packs next to the conserved A37. The conserved G41 and T44 residues of S1 interact with conserved A159 of S5 in all models. These conserved interactions may help anchor the domains together.

Another modeling criterion is that residue positions within transmembrane segments that are poorly conserved, but consistently hydrophobic among closely related proteins, will likely be exposed to lipids. This criterion is satisfied for the NaChBac family in S1 at residue positions T28, I30, A31, F35, I39, and I42 that reside on the same face of the S1 helix (see Fig. 2 of our accompanying study). This relatively narrow face is exposed to lipids in the adjusted models.

The VSD is linked to the PD by the L4–5 helix. Voltage-dependent conformational changes of the VSD are proposed to be coupled to the S6 activation gate primarily through interactions with L4–5, as proposed previously by Long et al.

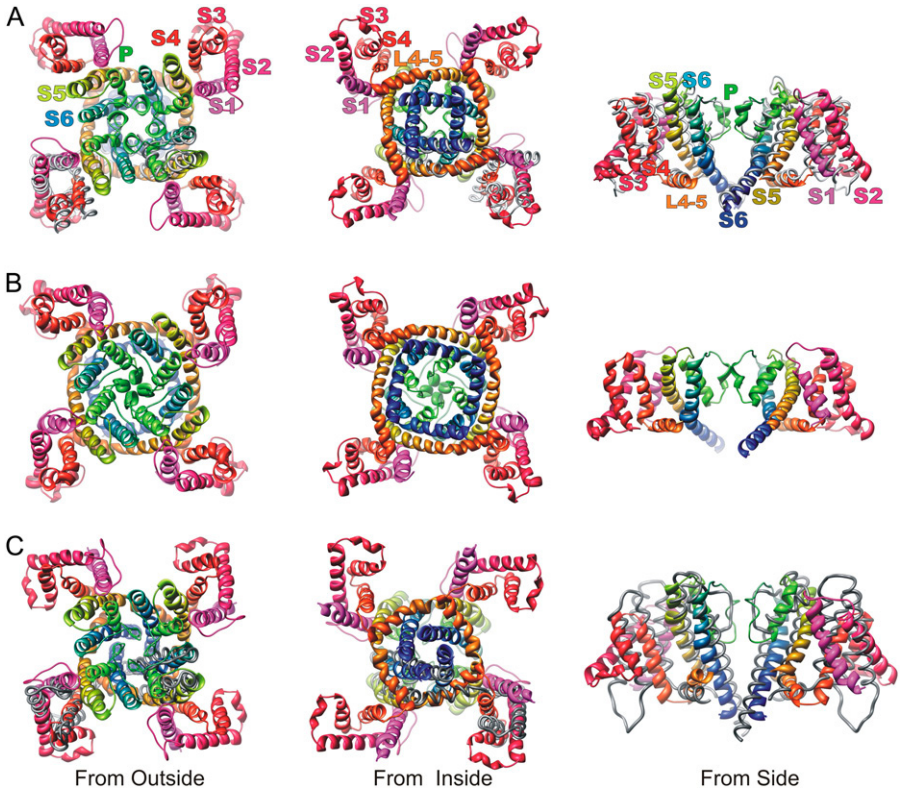

FIGURE 5 Ribbon representations of $Open_1$ (*A*), Open 2 (*B*), and $Closed_{0a}$ (*C*) models, as viewed from the outside (*left column*), inside (*middle column*), and side (*right column*). Side view shows only two VSDs and their interactions with the PD of two adjacent subunits. Structures are colored according to a spectrum beginning with magenta for S1, and ending with blue for S6 (see segment label colors in *A*). The Kv1.2 template structure is shown as a gray tube for one lower subunit in the top and bottom views of the $Open_1$ model, and for two subunits for side views. The MlotiK template is superimposed on the $Closed_{0a}$ model in a similar manner in *C*.

(17) for Kv1.2. The L4–5 helix is positioned between the N-termini of adjacent S5 segments. Modeling the L4–5 segment that links S4 to S5 was simple for the $Open_1$ model because no indels occur in this region. The L4–5 helix of the $Open_2$ model was modeled initially by changing the hinge between L4–5 and S5, to move the N-terminus of L4–5 near the end of the translocated S4 in a manner that maintained the orientation of the amphipathic L4–5 helix relative to the lipid surface, i.e., the hydrophilic face was kept in contact with water, whereas the hydrophobic face was kept in contact with lipid. Overall, the backbone structure of the $Open_1$ conformation remained quite similar to those of the Kv1.2 and Kv1.2/2.1 crystal structures throughout multiple simulations (see Fig. 5 for comparison of final model and Kv1.2/2.1 template). However, the backbone structure of the $Open_2$ model deviated more from the template structures of both domains during the first few MD simulations. The major change for the PD was an expansion of the inner pore region. This expansion was attributable to radially outward movements of the L4–5 helix, the N-terminus end of S5, and the C-terminus end of S6.

The L4–5 helix has a similar conformation in the closed models, but it is located nearer the axis of the pore. The hydrophobic face of L4–5 extends into the alkyl phase of the membrane, whereas its hydrophilic face is in the cytoplasm. It is packed tightly against S6 at the region where S6 becomes an amphipathic helix (the polar face of the C-terminus end of S6 starts just below where L4–5 crosses). The tight packing of the C-terminus portion of S4 on the opposite side of L4–5 in the $Closed_{0a}$ model may help hold it in place, thus preventing opening of the S6 gate. The models of the PD developed from KcsA and MlotiK structures differed primarily in their L4–5 and S5 regions. In both models, the positions of L4–5 and S5 shifted systematically in all four subunits during multiple simulations, i.e., the outer portion of S5 shifted radially outwardly, the tilt increased, and the L4–5 segment moved radially outward and upward into the lipid phase. Systematic changes also occurred in the VSD during MD simulations: the tilt of S2 increased, and the S2-S3 loop moved farther into the transmembrane region. Similar shifts occurred during MD simulations of the MlotiK crystal structure. We do not know whether these shifts indicate that the membrane-bound structure of MlotiK differs from the crystal structure, or if the MD simulation protocol distorted the correct structure. The closed models illustrated here are those developed from simulations of MlotiK-like homology models.

Consistency of NaChBac models with biotin/avidin results from KvAP

Previous LRET studies suggest that the open conformations of NaChBac and KvAP channels are similar (22). Ruta et al. (29) attached biotin adducts with tether lengths of 1 Å, 10 Å, and 17 Å to cysteines introduced in S1, S2, S3, S4, S5, and S6. The binding of the biotin adducts to either intracellular or extracellular avidin was then analyzed. The advantage of this approach is that the distance of the residue from the membrane surfaces, or center of the membrane, can be estimated

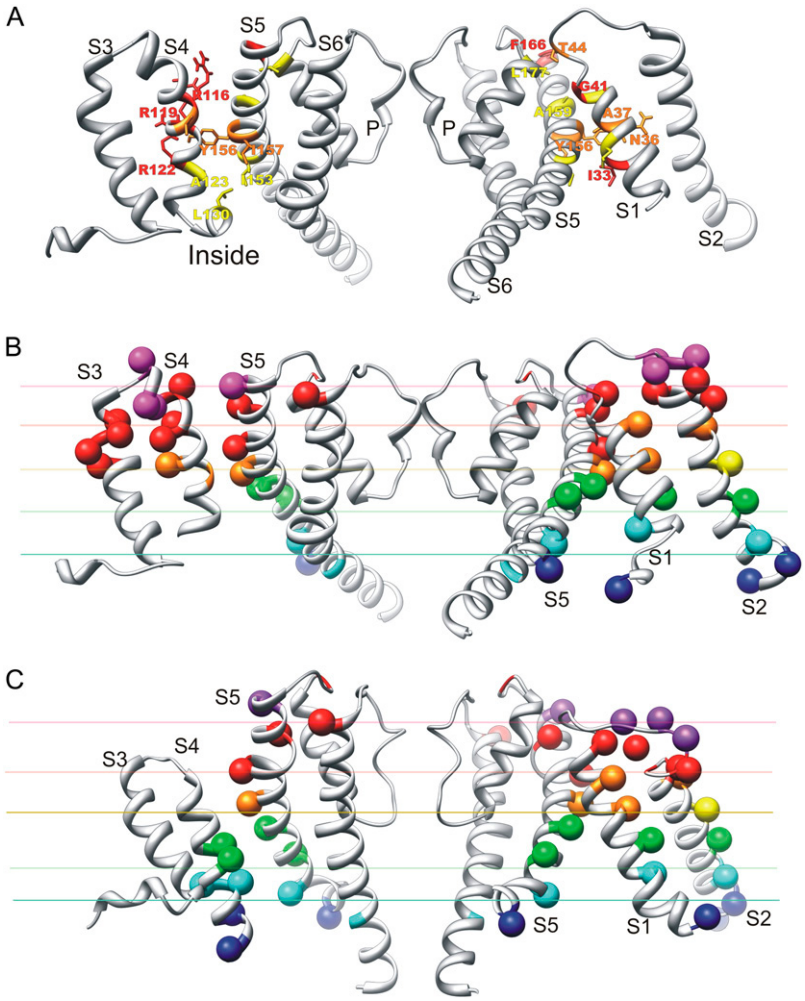

FIGURE 6 Side view of interactions between the VSD and PD of adjacent subunits: S1 and S2 are illustrated at right, and S3 and S4 at left. (*A*) Highly conserved residues involved in interactions between domains in the $Open_2$ model are labeled and colored by mutability, as in Fig. 2 of our accompanying study. Note that the Y156 side chain of S5 is inserted between S1 and S4 of the VSD, where it interacts with N36 and A37 of S1 and arginines of S4. (*B*) $Open_2$ model indicates residues analogous to those in KvAP, where biotin adducts with tethers of differing length bind to either intracellular or extracellular avidin. None of the biotin adducts can reach avidin on either side of the membrane for the yellow residue on S2. Adducts with 17-Å tethers can bind to avidin from the outside (*orange*) or inside (*green*) positions, but adducts with shorter tethers cannot. Adducts with 10-Å tethers can bind from the outside (*red*) or inside (*cyan*), but those with 1-Å tethers cannot. Adducts with 1-Å tethers can bind to avidin from the outside (*magenta*) or inside (*blue*). Colored lines approximate boundaries between residue categories. Alignment 1 of Fig. 2 was used to identify analogous NaChBac residues for S4. (*C*) Similar representation for the $Closed_{0a}$ model. Alignment 2 was used for S4.

because the avidin protein cannot enter the transmembrane region. The disadvantages are the long exposure times and virtually irreversible nature of the binding, which do not allow a direct determination of the voltage dependency of the binding. However, the results can be used to determine the extreme positions over time of residues relative to the two membrane surfaces. Segment S4 is the only one with residue positions where adducts accessible from the inside overlap those accessible from the outside. This finding indicates that S4 moves much more in the transmembrane direction than do the other segments.

These results are mapped onto the $Open_2$ and $Closed_{0a}$ models of NaChBac in Fig. 6, *B* and *C*. Interpretation of these data is predicated on assumptions that the adducts have an unimpeded path to the membrane surfaces, that soluble parts of the channel protein do not impede the ability of avidin to bind to the biotin adduct, and that binding of the adduct does not alter the conformation of the protein or its ability to reside in the conformation that would place the adduct nearest one of the surfaces. These conditions are probably best satisfied for S2, because it is the most peripheral segment and adducts were attached at positions on its outer, lipid-exposed face. The consistency of these results with the models is very good, considering the differences between sequences, that the NaChBac models were not adjusted to fit these data, and that the assumptions listed above may not always be valid. Each color (or category) of residue tends to reside within a given layer, designated by the colored lines (in Fig. 6, *B* and *C*). In both models, the yellow residue (for which no adducts bind to avidin) on S2 is located in the middle of the transmembrane region, between the orange and green residues (for outwardly and inwardly accessible adducts with 17-Å tethers only) of other segments. This result indicates that S2 does not undergo much transmembrane movement, and that the 17-Å adduct spans less than half of the bilayer when it binds to avidin. The consistency of the models with these data supports the proposed positioning within the transmembrane region of the VSD relative to the PD. The S4 segment is colored only for those positions for which adducts are accessible from the outside for the $Open_2$ model, and from the inside for the $Closed_{0a}$ model. Data for S4 agreed best with those of the other segments when alignment 1 of Fig. 2 is used for the $Open_2$ model, and alignment 2 is used for the $Closed_{0a}$ model. This is the opposite of those alignments that were used for NaChBac

with Kv1.2 and *Shaker*. These results suggests that S4 moves farther, by ~1 helical screw step, in KvAP than in NaChBac, and that S4 moves ~1 helical screw step farther in NaChBac than in Kv1.2 or *Shaker*. The data are satisfied equally well by the $Closed_{0b}$ model (not shown).

CONCLUSIONS AND DISCUSSION

Here we added a new twist to an old model. For over two decades, our laboratory has proposed that the movement of S4 during activation involves a helical screw mechanism. However, this mechanism may be more dynamic and complicated than first envisioned, e.g., S4 may have an elastic property that involves transitions between the α-helix and 3_{10} secondary structures during gating. There are several reasons to propose this new component for S4 transitions: 1), models in which the N-terminus portion of S4 has a 3_{10} structure in a closed conformation, whereas the C-terminus portion has a 3_{10} conformation in an open conformation, are based on the only crystal structures of 6 transmembrane segments superfamily of channels in apparently native-like closed and open/inactivated conformations; 2), the S3-S4 loop can be positioned nearer the extracellular surface if the N-terminus region has a 3_{10} structure; and 3), the elastic model appears to be more consistent with results of numerous experiments performed on *Shaker* channels. Long 3_{10} helices are rare, and their presence at different positions in Kv1.2/2.1 and the MlotiK structure led to speculations by crystallographers that 3_{10} helices may be important for gating (6–16). Here we present the first atomically explicit models of how transitions between α and 3_{10} conformations could be involved in activation gating.

Experimental estimates for the magnitude of transmembrane movement of S4 range from <2 Å (28) up to ~20 Å (29). The models proposed here suggest explanations for some of these apparently contradictory experimental findings. One contributing factor may involve the magnitude of movement of S4 differing among voltage-gated channels. Our working hypothesis is that in NaChBac, S4 moves farther (up to one helical screw step more) than in *Shaker* or Kv1.2, but not as far as S4 of the KvAP (~1 helical screw step less). This may help explain why some experiments performed on *Shaker* channels detect little transmembrane movement of S4, whereas other experiments performed on KvAP channels detect large transmembrane movements. This possibility creates an unusual situation in which it may be appropriate to use different sequence alignments for S4 for depolarized and hyperpolarized conformations. This possibility, and the possibility that the magnitude of the movement of S4 may be affected by the lengths of S3–S4 and S4–S5 linkers, are discussed in the Appendix. Another contributing factor to differing estimates of S4 movement may involve changes in the secondary structure of S4. Consider, for example, the putative elastic transition between the $Closed_{1b}$ and $Open_1$ models in Fig. 3. Probes attached to the N-terminus would detect little transmembrane movement, but would detect rotational movement of ~45°. In contrast, probes attached to the midregion would detect substantial transmembrane movement, but little rotational movement. Likewise, for the transition from the $Closed_{0b}$ to $Open_2$ configurations, Q107 at the beginning of S4 moves outwardly by <7 Å, whereas R122 (*R4*) moves outwardly by ~15 Å. Previous LRET studies of *Shaker* channels that detected little translational motion involved probes attached to the S3-S4 loop and the N-terminus of S4 (28), whereas the biotin/avidin experiments in KvAP that detected large movements (29) involved adducts attached to the midregion that are accessible from the outside in depolarized conformations, and from the inside in hyperpolarized conformations. A third contributing factor may involve a thermodynamic equilibrium among several conformations at negative voltages; different methods may be biased toward different conformations. For example, because of the irreversible nature of the binding of biotin to avidin, results from experiments using these probes likely reflect the extreme innermost and outermost positions of S4, even if those positions do not correspond to the most prevalent conformation. In contrast, studies in which LRET probes were attached to the N-terminus region may be biased toward conformations for which S4 has a more outward location, as described here regarding *Shaker* studies.

Uncertainties about the position of S4 in the resting conformations of K_v channels are reflected in models of Kv1.2 proposed by Pathak et al. (15) and Long et al. (6). As in our models, S4 in these models must be rotated about and translated along its axis to move it as a rigid body from the putative open conformation of the Kv1.2 or Kv1.2/2.1 chimera crystal structures to the modeled resting conformations, but its transmembrane movement is shorter in the model of Pathak et al. (15) (~8 Å) than in the model of Long et al. (6) (~15 Å). In the resting-conformation Kv1.2 model of Pathak et al. (15), *R2* is located near the position of the arginine in Fig. 4 *A*, and *R1* is located well above the transition barrier, where it binds to *E2a*. On the other hand, in the Kv1.2 model in Fig. 6 of Long et al. (6), *R1* is positioned well below the transition barrier in the resting conformation, where it binds to *E2b*. We favor an intermediate location, with *R1* positioned within the transition barrier for the innermost conformation, as we described regarding NaChBac and *Shaker* models. However, we also suspect that thermodynamic fluctuations lead to the formation of other conformations for which *R1* is farther out at resting voltages.

Some uncertainty also exists about the position of S4 in the open conformation of NaChBac. Here we developed two models for the open conformation. Although the $Open_1$ model is more like the Kv1.2/2.1 crystal structure, the $Open_2$ model is more consistent with the LRET and gating current data. According to our working hypothesis, a Kv1.2-like $Open_1$ conformation may occur, but probably as a transition conformation between the principal closed and open conformations.

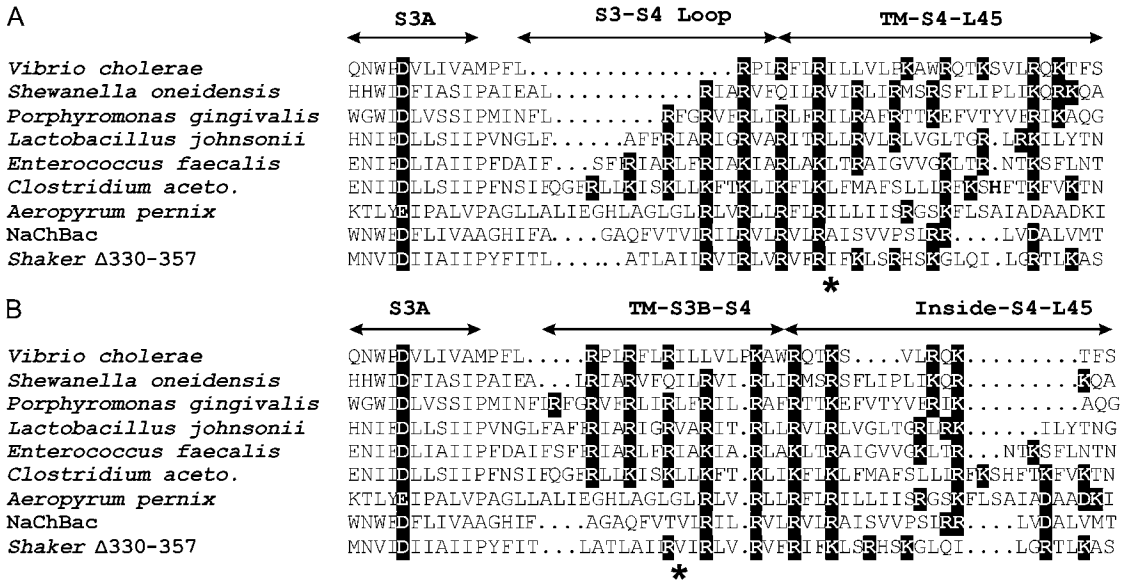

FIGURE 7 Tentative structural alignments for a series of channels with variable lengths of S3–S4 and S4–S5 linkers in open (*A*) and resting (*B*) conformations. Charged residues have black backgrounds. Gating charge attributable to S4 residues can be approximated by the number or positively charged residues that pass the transition barrier (indicated by *asterisk*) for the transition between open and resting. Lengths of S4–S5 linkers are similar for resting conformation alignments, and lengths of S3–S4 linkers are similar for open conformation alignments. The first seven sequences are designated by the prokaryote in which they are encoded. In these alignments, the lengths of S3–S4 are more variable in open conformations, whereas the lengths of L4–5 linkers are more variable in resting conformations.

Suggestions for experiments to test the models presented here are listed in the Supplementary Material (Fig. S1).

APPENDIX

We proposed previously that the magnitude of the movement of S4 may vary among different voltage-gated channels, and that the magnitude of this movement may be affected by the lengths of the S3–S4 and possibly S4–S5 linkers (9). If so, then the structural alignment between two channels may differ for open and resting conformations. The four-helical-screw-step motion of S4 proposed here appears to be the maximum allowable by the relatively short linkers of NaChBac. This conclusion is based on our finding that for NaChBac models in which S4 was placed one helical screw step farther out (a position similar to that of S4 in the KvAP crystal structure), MD simulations caused S4 to move inwardly back to a position near that of the $Open_2$ model. Moving S4 farther inward than in the $Closed_{0a}$ model would remove most of S4 from the transmembrane region, and would place the S3-S4 loops and the ends of the S3 and S4 helices farther inside the transmembrane region, where the exposure of helix termini to lipid alkyl chains (or distorting the lipids so that the termini would interact with headgroups and water) would likely be energetically unfavorable. Gonzalez et al. (30) found that the S3–S4 linker of *Shaker* channels can be made 28 residues shorter (Δ330–357) without altering the voltage dependency of activation gating, but that longer deletions alter the voltage dependency. The linker in the Δ330–357 mutant is one residue longer than for NaChBac (Fig. 7). This similarity would suggest that S4 in the two channels should be able to move about the same distance. Although the NaChBac S3–S4 linker is considered to be short, this linker is up to 13 residues shorter in some prokaryotic K^+ channel sequences. We classify prokaryotic channels with an S2–S3 linker that is two residues shorter than those of NaChBac and Kv1.2 into a family to which KvAP belongs. The lengths of the S3–S4 and S4–S5 linkers vary greatly within this family, most often in increments of three residues (Fig. 7). Although KvAP has one of the longest sets of linkers within this family, the shortest linkers are a total of 20 residues shorter. Fig. 7 illustrates two plausible alignments for the S4 segments of some of these sequences: one for the depolarized open/desensitized conformation, and one for a hyperpolarized resting conformation. The S4 segments of those like KvAP with linkers longer than those of NaChBac could move farther than those of NaChBac, but those with shorter linkers should not move as far. The differences in the two alignments should reflect the differences in the magnitude of S4 movement, e.g., the two alignments between NaChBac and the sequence from *Vibrio cholerae* differ by 12 positions, suggesting that the movement of S4 for NaChBac could be four helical screw steps farther than for channels with the shortest linkers, implying that S4 does not move much in channels with the shortest linkers. This does not necessarily mean that these channels could not gate in a voltage-dependent manner, e.g., the elastic transition from the MlotiK-like $Closed_{1b}$ to the Kv1.2-like $Open_2$ model involves little translational movement of the N-terminus of S4. Channels with short linkers might be good candidates for crystal structures, because of the possibility that fewer conformational states would lead to greater stability of the protein.

SUPPLEMENTARY MATERIAL

To view all of the supplemental files associated with this article, visit www.biophysj.org.

We thank Benoit Roux for providing the script to calculate the gating charge, and Adina Milac and Sijung Yun for comments on the manuscript.

This work was supported by the Intramural Research Program of the Center for Cancer Research, National Cancer Institute, National Institutes of Health.

REFERENCES

1. Hodgkin, A. L., and A. F. Huxley. 1952. A quantitative description of membrane current and its application to conduction and excitation in nerve. *J. Physiol.* 117:500–544.

2. Noda, M., S. Shimizu, T. Tanabe, T. Takai, T. Kayano, T. Ikeda, H. Takahashi, H. Nakayama, Y. Kanaoka, and N. Minamino. 1984. Primary structure of *Electrophorus electricus* sodium channel deduced from cDNA sequence. *Nature*. 312:121–127.

3. Guy, H. R., and P. Seetharamulu. 1986. Molecular model of the action potential sodium channel. *Proc. Natl. Acad. Sci. USA*. 83:508–512.

4. Guy, H. R. 1988. A model relating the structure of the sodium channel to its function. *In* Current Topics in Membranes and Transport. W. Agnew, T. Claudio, and F. Sigworth, editors. Academic press, New York. 289–308.

5. Jiang, Y., A. Lee, J. Chen, V. Ruta, M. Cadene, B. T. Chait, and R. MacKinnon. 2003. X-ray structure of a voltage-dependent K^+ channel. *Nature*. 423:33–41.

6. Long, S. B., X. Tao, E. B. Campbell, and R. MacKinnon. 2007. Atomic structure of a voltage-dependent K^+ channel in a lipid membrane-like environment. *Nature*. 450:376–382.

7. Durell, S. R., Y. Hao, and H. R. Guy. 1998. Structural models of the transmembrane region of voltage-gated and other K^+ channels in open, closed, and inactivated conformations. *J. Struct. Biol.* 121:263–284.

8. Durell, S. R., I. H. Shrivastava, and H. R. Guy. 2004. Models of the structure and voltage-gating mechanism of the *Shaker* K^+ channel. *Biophys. J.* 87:2116–2130.

9. Shrivastava, I. H., S. R. Durell, and H. R. Guy. 2004. A model of voltage gating developed using the K_vAP channel crystal structure. *Biophys. J.* 87:2255–2270.

10. Schoppa, N. E., K. McCormack, M. A. Tanouye, and F. J. Sigworth. 1992. The size of gating charge in wild-type and mutant *Shaker* potassium channels. *Science*. 255:1712–1715.

11. Aggarwal, S. K., and R. MacKinnon. 1996. Contribution of the S4 segment to gating charge in the *Shaker* K^+ channel. *Neuron*. 16:1169–1177.

12. Seoh, S. A., D. Sigg, D. M. Papazian, and F. Bezanilla. 1996. Voltage-sensing residues in the S2 and S4 segments of the *Shaker* K^+ channel. *Neuron*. 16:1159–1167.

13. Kuzmenkin, A., F. Bezanilla, and A. M. Correa. 2004. Gating of the bacterial sodium channel, NaChBac: voltage-dependent charge movement and gating currents. *J. Gen. Physiol.* 124:349–356.

14. Chanda, B., O. K. Asamoah, R. Blunck, B. Roux, and F. Bezanilla. 2005. Gating charge displacement in voltage-gated ion channels involves limited transmembrane movement. *Nature*. 436:852–856.

15. Pathak, M. M., V. Yarov-Yarovoy, G. Agarwal, B. Roux, P. Barth, S. Kohout, F. Tombola, and E. Y. Isacoff. 2007. Closing in on the resting state of the *Shaker* K(+) channel. *Neuron*. 56:124–140.

16. Clayton, G. M., S. Altieri, L. Heginbotham, V. M. Unger, and J. H. Morais-Cabral. 2008. Structure of the transmembrane regions of a bacterial cyclic nucleotide-regulated channel. *Proc. Natl. Acad. Sci. USA*. 105:1511–1515.

17. Long, S. B., E. B. Campbell, and R. MacKinnon. 2005. Crystal structure of a mammalian voltage-dependent *Shaker* family K^+ channel. *Science*. 309:897–903.

18. Burley, S. K., and G. A. Petsko. 1985. Aromatic-aromatic interaction: a mechanism of protein structure stabilization. *Science*. 229: 23–28.

19. Killian, J. A., and G. von Heijne. 2000. How proteins adapt to a membrane-water interface. *Trends Biochem. Sci*. 25:429–434.

20. Ahern, C. A., and R. Horn. 2005. Focused electric field across the voltage sensor of potassium channels. *Neuron*. 48:25–29.

21. Blanchet, J., S. Pilote, and M. Chahine. 2007. Acidic residues on the voltage-sensor domain determine the activation of the NaChBac sodium channel. *Biophys. J.* 92:3513–3523.

22. Richardson, J., R. Blunck, P. Ge, P. R. Selvin, F. Bezanilla, D. M. Papazian, and A. M. Correa. 2006. Distance measurements reveal a common topology of prokaryotic voltage-gated ion channels in the lipid bilayer. *Proc. Natl. Acad. Sci. USA*. 103:15865–15870.

23. Li, L., I. Vorobyov, A. D. MacKerell, Jr., and T. W. Allen. 2008. Is arginine charged in a membrane? *Biophys. J.* 94:L11–L13.

24. Campos, F. V., B. Chanda, B. Roux, and F. Bezanilla. 2007. Two atomic constraints unambiguously position the S4 segment relative to S1 and S2 segments in the closed state of *Shaker* K channel. *Proc. Natl. Acad. Sci. USA*. 104:7904–7909.

25. Larsson, H. P., O. S. Baker, D. S. Dhillon, and E. Y. Isacoff. 1996. Transmembrane movement of the *Shaker* K^+ channel S4. *Neuron*. 16:387–397.

26. Tombola, F., M. M. Pathak, and E. Y. Isacoff. 2005. Voltage-sensing arginines in a potassium channel permeate and occlude cation-selective pores. *Neuron*. 45:379–388.

27. Tombola, F., M. M. Pathak, P. Gorostiza, and E. Y. Isacoff. 2007. The twisted ion-permeation pathway of a resting voltage-sensing domain. *Nature*. 445:546–549.

28. Posson, D. J., P. Ge, C. Miller, F. Bezanilla, and P. R. Selvin. 2005. Small vertical movement of a K^+ channel voltage sensor measured with luminescence energy transfer. *Nature*. 436:848–851.

29. Ruta, V., J. Chen, and R. MacKinnon. 2005. Calibrated measurement of gating-charge arginine displacement in the K_vAP voltage-dependent K^+ channel. *Cell*. 123:463–475.

30. Gonzalez, C., F. J. Morera, E. Rosenmann, O. Alvarez, and R. Latorre. 2005. S3b amino acid residues do not shuttle across the bilayer in voltage-dependent *Shaker* K^+ channels. *Proc. Natl. Acad. Sci. USA*. 102:5020–5025.